Applied Catalysis B: Environmental 142–143 (2013) 315–322

Contents lists available at SciVerse ScienceDirect

Applied Catalysis B: Environmental

journal homepage: www.elsevier.com/locate/apcatb

Kinetic behaviour of catalysts with different CuO-ZnO-Al_2O_3 metallic function compositions in DME steam reforming in a fluidized bed

Javier Ereña*, Jorge Vicente, Andrés T. Aguayo, Martin Olazar, Javier Bilbao, Ana G. Gayubo

Departamento de Ingeniería Química, Universidad del País Vasco UPV/EHU, Apartado 644, 48080 Bilbao, Spain

ARTICLE INFO

Article history:
Received 11 March 2013
Received in revised form 10 May 2013
Accepted 16 May 2013
Available online 23 May 2013

Keywords:
SRD
Dimethyl ether
Reforming
Hydrogen production
Catalyst preparation

ABSTRACT

The effect of CuO-ZnO-Al_2O_3 (CuZnAl) metallic function composition on kinetic behaviour has been studied in the steam reforming of dimethyl ether (SRD), for bifunctional catalysts synthesized using this metallic function (with different formulations) and a HZSM-5 zeolite modified by treating it with NaOH in order to moderate acidity. The kinetic performance of the catalysts has been determined by experimentation in a fluidized bed reactor in the 225–325 °C range, and the reaction indices (dimethyl ether (DME) and methanol conversions and H_2 and CO yields) have been explained based on the physico-chemical properties of the metallic and acid functions and of the bifunctional catalyst.

The catalyst prepared by wet physical mixing with a mass ratio of 1:1 between the metallic function (CuZnAl, with Cu/Zn/Al atomic ratio = 4.5:4.5:1.0) and the acid one, allows obtaining high values of DME conversion and H_2 yield in the 275–300 °C range by minimizing the CO formation rate and deactivation by coke, which is explained by the high dispersion of Cu on the metallic function and the moderate acid strength of the HZSM-5 zeolite modified by alkaline treatment. Although coke content in the catalyst is low, it is mainly deposited on the metallic function, causing a decrease in methanol conversion with time on stream.

1. Introduction

Dimethyl ether (DME) is available for use as fuel and raw material (alternative to methanol) for hydrocarbon production and, furthermore, for use as H_2 vector in proton exchange membrane fuel cells (PEMFC), thanks to its high hydrogen content (13 wt% of DME vs. 12.5 wt% of methanol), low toxicity (harmless), liquid-storage density, non-corrosiveness and similar infrastructure requirements as for handling LPG [1,2]. Furthermore, the steam reforming of DME (SRD) can also proceed at low temperatures, similarly to the steam reforming of methanol (SRM) [3–10].

Furthermore, single-step DME synthesis (on bifunctional catalysts) is one of the routes with a higher potential for upgrading (via syngas) alternative raw materials to oil and especially for biomass upgrading. The integration of methanol synthesis and its dehydration into a single step involves significant thermodynamic advantages over the two-step process (methanol synthesis and its subsequent dehydration to DME), which enhances CO_2 co-feeding with syngas and the use of a syngas raw material with a lower H_2/CO ratio than that required for methanol synthesis [11–15]. Therefore, DME synthesis is considered as a key process for CO_2 sequestration [16] and the viability of lignocellulosic biomass gasification [17].

The SRD process consists of two steps in series:

DME hydrolysis (on the acid function in the catalyst):

$$(CH_3)_2O + H_2O \leftrightarrow 2CH_3OH \quad (1)$$

MeOH steam reforming (on the metallic function):

$$CH_3OH + H_2O \leftrightarrow 3H_2 + CO_2 \quad (2)$$

$$\text{Overall reaction}: (CH_3)_2O + 3H_2O \leftrightarrow 6H_2 + 2CO_2 \quad (3)$$

Besides, the reverse water-gas shift reaction (r-WGS) takes place over the metallic function:

$$CO_2 + H_2 \leftrightarrow H_2O + CO \quad (4)$$

Methane can also be generated via DME decomposition, when a strong acid catalyst or high reforming temperatures are used [18]:

$$(CH_3)_2O \rightarrow CH_4 + H_2 + CO \quad (5)$$

* Corresponding author. Tel.: +34 94 6015363; fax: +34 94 6013500.
E-mail address: javier.erena@ehu.es (J. Ereña).

0926-3373/$ – see front matter © 2013 Elsevier B.V. All rights reserved.
http://dx.doi.org/10.1016/j.apcatb.2013.05.034

Nomenclature

A0.2-300	HZSM-5 zeolite treated with 0.2 M NaOH for 300 min
1Cu1Zn, 2Cu1Zn, CZA	CuZnAl metallic functions prepared in the laboratory (Cu/Zn/Al nominal atomic ratios = 1.0:1.0:0, 2.0:1.0:0 and 4.5:4.5:1.0, respectively)
$\bar{d}_{Cu}$, $\bar{d}_{CuO}$	average particle size of Cu and of CuO, Å
d_{pore}	pore diameter, Å
F_i, $F_{i,0}$	molar flow rate of i component at the reactor outlet and in the feed, respectively
G66	CuZnAl commercial metallic function (Cu/Zn/Al nominal atomic ratio = 3.0:1.0:1.0)
P_{DME}	DME partial pressure, bar
P_{H_2}	H_2 production, $mmol_{H_2}/(h\ g_{catalyst})$
S_{BET}	BET surface area of the solid, m^2/g
$S_{metallic}$	specific metal surface area, $m^2{}_{Cu}/g_{Cu}$
$S_{micropore}$	micropore surface area, m^2/g
$V_{mesopore}$, $V_{micropore}$	mesopore and micropore volume, cm^3/g
W	catalyst weight, g
X_{DME}	DME conversion
x_i	i component molar fraction
X_{MeOH}	methanol effective conversion in the second step of the SRD process
Y_i	yield of i component
υ_i	stoichiometric coefficient of i component

Moreover, the conversion of methanol and DME into hydrocarbons can take place at temperatures above 300 °C on strong acid sites [19], and significant coking may occur on the catalyst surface due to the dehydrogenation of the hydrocarbons formed [20]:

$$\text{Oxygenates} \rightarrow \text{hydrocarbons} \rightarrow \text{coke} \quad (6)$$

A suitable catalyst must be used to attain high yields of H_2, given that: (i) steps shown in Eqs. (1) and (2) must be sufficiently high and well-matched and (ii) steps shown in Eqs. (4)–(6) should be minimized, thereby reducing the production of coke (deactivates the SRD catalyst) and CO (poisons the fuel cell anode).

γ-Al_2O_3 is commonly used as an acid function for DME hydrolysis, Eq. (1), although it is of low activity and stability due to its high hydrophilic nature [11,21]. Activity for hydrolysis has been increased by the direct one-pot synthesis process, which generates a homogeneous mesoporous structure, and by adding Ga_2O_3 and d-block transition metals (Ni, Cu, Zn), thus obtaining a high level of acidity and suitable electronic structure for DME reforming, with H_2 yields being in the 0.77–0.80 range at 350 °C, with great stability [3,22].

Furthermore, the metallic functions used have Cu as the main active component for methanol reforming, Eq. (2), although noble metals (Pt, Ru, Rh, Au) have also been used [23–25]. ZnO is the usual promoter suitable for enhancing the surface dispersion of Cu [26,27], with the usual metal supports being Al_2O_3 and CeO_2.

The CuO-ZnO-Al_2O_3 (CuZnAl) metallic function and the HZSM-5 zeolite (widely studied for DME synthesis and SRM) have been commonly used in the catalysts for SRD [23,28–31], which is due to both the high activity of the HZSM-5 zeolite for DME hydrolysis and the contrasted capacity of the CuZnAl metallic function for methanol reforming [28].

A previous paper analyses the role of the acid function and confirms the interest of modifying the HZSM-5 zeolite properties by treating with NaOH (desilication) in order to minimize the formation of hydrocarbons and coke (Eq. (6)) [32]. The contribution this paper makes is the systematic study of the effect the formulation of CuZnAl metallic functions (Cu/Zn ratio and Al_2O_3 presence) has on their properties and, therefore, on their kinetic performance. Special attention has been paid to the methanol reforming step, Eq. (2), as well as to catalyst stability.

2. Experimental

2.1. Catalyst preparation

The metallic functions with different Cu/Zn/Al atomic ratio have been prepared by the conventional coprecipitation method [33,34]. Sodium carbonate ($Na_2CO_3{\cdot}10H_2O$ (*Panreac*, 99%)) is used to precipitate the corresponding metallic nitrates ($Cu(NO_3)_2{\cdot}3H_2O$, $Zn(NO_3)_2{\cdot}6H_2O$ and $Al(NO_3)_3{\cdot}9H_2O$, (*Panreac*, 99%)), as it is the best agent for coprecipitating metallic components and for a suitable pH control [35]. The precipitation step is performed at 70 °C with constant pH (6.8–7.2), followed by a one-hour ageing period (under the same conditions of pH and temperature). The resulting solid is washed (as often as required for the total removal of alkaline cations), dried in two steps (at room temperature for 12 h and then at 110 °C for another 12 h) and calcined (*Thermicon P Heraeous*, *SA* muffle) at 325 °C for 3 h, following a heating ramp of 5 °C/min in order to transform the metallic carbonates (precursors) into oxides.

The metallic functions have been denoted 2Cu1Zn, 1Cu1Zn and CZA (based on their Cu/Zn/Al nominal atomic ratios, which are 2.0:1.0:0, 1.0:1.0:0 and 4.5:4.5:1.0, respectively). The results obtained with these metallic functions have been compared with those of a commercial catalyst for methanol steam reforming supplied by *Süd Chemie* in the form of small pellets (6 mm × 4.75 mm) ($CuO/ZnO/Al_2O_3$ molar ratio = 6.0:2.1:1.0), denoted G66 (with Cu/Zn/Al atomic ratio = 3.0:1.0:1.0).

The acid function is a ZSM-5 zeolite obtained by treating a commercial ZSM-5 zeolite (SiO_2/Al_2O_3 = 30, *Zeolyst International*) supplied in ammonium form, with a 0.2 M solution of NaOH (*Panreac*, 99%), by stirring at 80 °C for 300 min, using a reflux condenser to prevent evaporation. The sodium ZSM-5 zeolite treated has been ion-exchanged with an ammonium nitrate solution, and subsequently washed and dried in air for 24 h at room temperature and then at 110 °C for another 24 h. The acid form is obtained after calcination (*Thermicon P Heraeous*, *SA* muffle) (3 h at 550 °C). The resulting zeolite has been called A0.2-300. The effect of NaOH treatment and zeolite properties is detailed elsewhere [32].

Wet physical mixing for contacting the metallic function with the acid one in the preparation of the bifunctional catalysts has consisted in slowly adding the calcined and ground acid function to 1 L of distilled water stirred at ambient temperature [36], until a white and well-dispersed suspension is attained. The calcined and ground (<60 μm) metallic function (synthesized by coprecipitation, as described above) is then slowly added and stirred for 30 min. The solid phase is separated by centrifugation and dried, firstly at ambient temperature for 24 h and then in an oven at 110 °C for 24 h. Based on the results in a previous paper, the mass ratio between the metallic and acid functions has been set at 1:1 [36].

The bifunctional catalysts obtained are calcined at 325 °C for 3 h. The powder obtained is pressed (*Herzog*) in the form of pellets (30 mm × 0.4 mm) and then ground and sieved (*CISA RP 200N*) to a size of 150–250 μm, which is a suitable for use in the fluidized bed reactor.

2.2. Catalyst characterization

The Cu/Zn/Al atomic ratio of the metallic functions has been determined by ICP-AES in an *ARL 3410* with Ar as carrier and plasma torch. The Si/Al ratio of the HZSM-5 zeolite has been determined

by X-ray fluorescence (XRF, *Philips MiniPal PW4025)*, according to the protocol described by Yusta et al. [37].

The physical properties of the metallic and acid functions and of the bifunctional catalysts have been determined by N_2 adsorption–desorption in a *Micromeritics ASAP 2010* and by Hg porosimetry in a *Micromeritics Autopore 9220*. The metallic species liable to reduction and the temperature triggering the reduction have been determined by temperature programmed reduction (TPR, *AutoChem 2920 from Micromeritics*) by passing a 50 cm^3/min stream with 10% volume of H_2 in Ar. The metal surface area and the size of the metal crystallite (in the metallic function of the bifunctional catalysts) have been determined by chemisorption using N_2O pulses (*Micromeritics AutoChem 2920* coupled to a *Balzers Instruments Omnistar* mass spectrometer via a thermostated line in order to analyze the amounts of both N_2 formed and unreacted N_2O by monitoring the signals corresponding to masses 28 and 44, respectively). Based on the volume of gas reacted, the active surface of Cu has been calculated from the adsorbate surface area ($1.63{\cdot}10^{19}$ at_{Cu}/m^2) and the adsorption stoichiometry (2 Cu atoms per oxygen atom) [38].

The crystallinity of the HZSM-5 zeolite has been determined by X-ray diffraction analysis in a *Philips PW 1710*. Total acidity and the acid strength distribution of the zeolite and of the bifunctional catalysts have been determined by calorimetric measurement of the differential adsorption (DSC) of NH_3 at 150 °C and subsequent temperature-programmed desorption (TPD) of adsorbed NH_3, with a ramp of 5 °C/min up to 550 °C. The equipment used is a *TA Instruments SDT 2960* thermobalance connected on-line to a *Balzers Instruments Thermostar* mass spectrometer [39,40]. Table 1 shows the values of the physical properties and acidity for the HZSM-5 zeolite (A0.2-300) used in the preparation of the bifunctional catalysts.

The coke content in the deactivated catalysts has been determined by combustion with air following a heating ramp of 5 °C/min from room temperature to 600 °C in a thermobalance (*TA Instruments SDT 2960*) connected on-line to a mass spectrometer (*Balzers Instruments Thermostar*) via a thermostated line in order to monitor the signals corresponding to the combustion gases (masses 14, 18, 28 and 44 corresponding to N_2, H_2O, CO and CO_2, respectively) [12,41]. The combustion cannot be monitored by thermogravimetry because Cu oxidation occurs in parallel with combustion, masking the thermogravimetric signal.

2.3. Reaction equipment and product analysis

The kinetic runs have been carried out in automated reaction equipment (*Microactivity Reference from PID Eng & Tech*) provided with an isothermal fluidized-bed reactor (22 mm of internal diameter and total length of 460 mm) connected on-line to a gas chromatograph (*Agilent Micro GC 3000*) for product analysis [36]. The hydrodynamic properties of the bed have been improved by mixing the catalyst (particle size between 150 and 250 μm) with an inert solid (CSi, particle size between 60 and 90 μm) at a catalyst/inert ratio of 1:4. The Micro-GC is provided with four modules for the analysis of: (1) permanent gases (O_2, N_2, H_2, CO, CH_4); (2) oxygenates (methanol, DME, CO_2), light olefins (C_2–C_3) and water; (3) C_2–C_6 hydrocarbons; (4) C_6–C_{12} hydrocarbons and oxygenate compounds. The compounds were quantified and identified using calibration standards of known concentration. The balance of atoms (C, H, O) is closed in all runs above 98%.

The operating conditions are as follows: total pressure, 1.2 bar; steam/DME/He molar ratio = 3:1:0.85 (or 4:1:0.55); space time, up to 0.60 $g_{catalyst}$ h/g_{DME}; temperature, between 225 and 325 °C. Prior to the runs, the catalyst is reduced at 300 °C for 2 h with a total flow rate of 60 ml/min of 10% H_2 in He.

3. Results and discussion

3.1. Effect of the metallic function Cu/Zn/Al atomic ratio on the catalyst properties

The Cu/Zn/Al atomic ratios of the synthesized metallic functions (determined by ICP-AES) have been as follows: 2.2:1.0:0 (for the 2Cu1Zn metallic function), 1.1:1.0:0 (for 1Cu1Zn) and 4.5:4.7:1.0 (for CZA). These compositions are very close to the nominal values of 2.0:1.0:0, 1.0:1.0:0 and 4.5:4.5:1.0, respectively. The fact the composition is close to the nominal one means the coprecipitation method is suitable for obtaining a reproducible metallic function with the desired Cu/Zn/Al ratio. Furthermore, the commercial G66 catalyst used as reference has a Cu/Zn/Al atomic ratio of 3.0:1.0:1.0, according to the data provided by the supplier.

Fig. 1 shows the XRD diffractograms of the metallic functions: G66, 2Cu1Zn, 1Cu1Zn (all calcined at 325 °C), and CZA (calcined at 325 and 400 °C). Peaks are identified for CuO and ZnO crystalline phases (which is evidence of the full development of the structure corresponding to the oxides that make up the metallic function), as well as for the species corresponding to Cu, Zn and Al carbonates formed by using Na_2CO_3 as a coprecipitation agent [42]. Peaks characteristic of Al_2O_3 are not observed, which is probably due to Al_2O_3 low content in the samples and its high dispersion, although it may also be present in amorphous form [43]. The wider and weakly defined peaks for the CZA metallic function calcined at 325 °C are due to a high dispersion of the metallic function, which is consistent with the values for crystal size shown in Table 2, either for Cu metal particles (determined by pulsed N_2O chemisorption of reduced samples) or for CuO crystallites prior to reduction (determined from XRD peaks based on the equation by Debye-Scherrer). These results confirm that Zn contributes to dispersing Cu particles, thereby obtaining a smaller metallic particle size for the 1Cu1Zn function than for the 2Cu1Zn function.

Table 1
Properties of the HZSM-5 zeolite treated with NaOH (A0.2-300).

Physical properties					
Si/Al	S_{BET}, m^2/g	$S_{external}$, m^2/g	$S_{micropore}$, m^2/g	$V_{micropore}$, cm^3/g	$V_{mesopore}$, cm^3/g
13.0	466	176	290	0.12	0.30

Acid properties						
Total acidity, $mmol_{NH_3}$ / g	Average acid strength					
	DSC kJ / mol_{NH_3}	TPD				
		Weak sites		Strong sites		
		T_{max}, °C	$mmol_{NH_3}$ / g	T_{max}, °C	$mmol_{NH_3}$ / g	
0.71	120	263	0.45	409	0.26	

Table 2
Physical properties and metal surface area for the metallic functions (the values of temperature and time in the first column correspond to calcination temperature and duration).

Metallic function	S_{BET}, m^2/g	$V_{mesopore}$, cm^3/g	d_{pore}, Å	$S_{metallic}$, m^2_{Cu}/g_{Cu}	$\bar{d}_{Cu}$, Å	$\bar{d}_{CuO}$, Å
G66 (commercial)	83	0.35	155	78	86	53
Non-calcined CZA	55	0.19	168	–	–	–
Calcined at 300 °C, 3 h	119	0.48	136	155	43	–
325 °C, 3 h	113	0.49	143	141	48	36
400 °C, 4 h	77	0.43	194	76	88	72
Non-calcined 1Cu1Zn	40	0.18	146	–	–	–
Calcined at 325 °C, 3 h	73	0.29	162	76	89	89
400 °C, 4 h	35	0.25	287	38	176	–
Non-calcined 2Cu1Zn	20	0.08	234	–	–	–
Calcined at 325 °C, 3 h	70	0.28	156	64	104	99
400 °C, 4 h	35	0.15	200	25	266	–

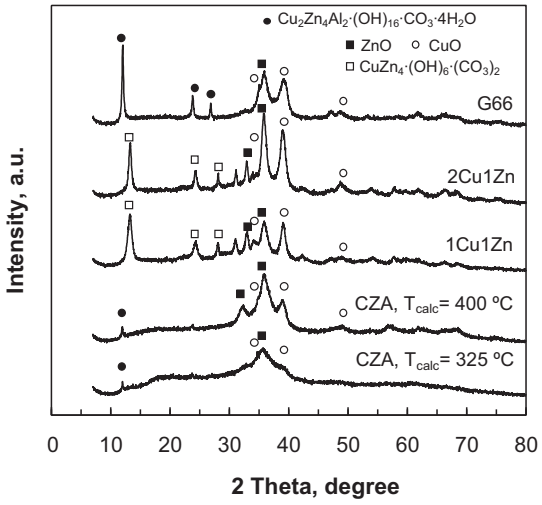

Fig. 1. XRD patterns for G66, 2Cu1Zn and 1Cu1Zn metallic functions (calcined at 325 °C) and CZA metallic function (calcined at 325 and 400 °C).

The TPR profiles of the metallic functions (Fig. 2) contain a prevailing peak corresponding to the reduction of Cu^{2+} to Cu^0 [44] together with overlapping peaks that may correspond to the reduction of the amorphous CuO phase to highly dispersed Cu [45] and, therefore, a high size heterogeneity is expected for Cu particles. Other authors attribute peak overlapping to the reduction in the hydroxycarbonated species of the metal precursor that have not undergone calcination [46]. The CZA metallic function calcined at 325 °C undergoes its maximum reduction at a higher temperature (190 °C) than the 2Cu1Zn and 1Cu1Zn metallic functions calcined at the same temperature. Furthermore, the corresponding peak is wider, which evidences a high interaction between Cu and Al_2O_3 attributed to the Cu^{2+} ions are in the Al lattice [3,22]. As the calcination temperature is higher (400 °C) the reduction peak shifts to a higher temperature (205 °C).

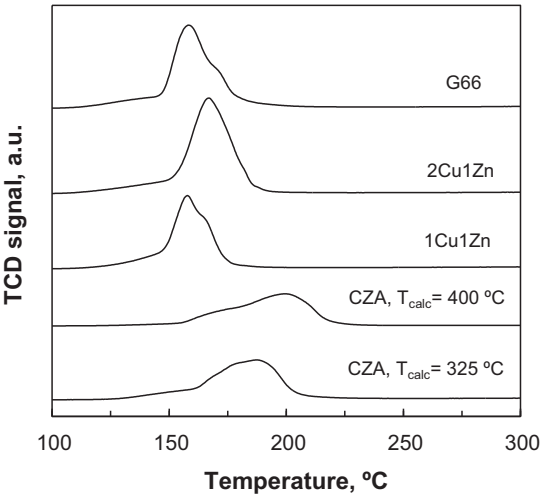

Fig. 2. TPR profiles for G66, 2Cu1Zn and 1Cu1Zn metallic functions (calcined at 325 °C) and CZA metallic function (calcined at 325 and 400 °C).

Table 2 shows the physical properties and metal surface area for the metallic functions calcined at different temperatures and for their metal precursors (Cu, Zn and Al hydroxycarbonates) prior to calcination. The precursors have a very low BET surface area and pore volume, but subsequent to calcination both parameters increase due to mesopore formation (caused by the release of CO_2 and H_2O throughout carbonate decomposition) in the 20–500 Å range, which are similar values to those reported in the literature [34,47]. An increase in the calcination temperature gives way to a decrease in the BET surface area and pore volume, but to an increase in the average pore size due to metal agglomeration that blocks the smaller pores. The similarity between the values of the BET surface area and pore volume corresponding to 1Cu1Zn and 2Cu1Zn functions evidences that promotion with Zn has a small influence on the physical properties of the metallic function. Nevertheless, the addition of a small amount of Al significantly increases the BET surface area and pore volume [48].

Furthermore, the results in Table 2 reveal that the specific metal surface area for 1Cu1Zn function is higher than that for 2Cu1Zn function, and the decrease in the specific metal surface area by increasing the calcination temperature (due to Cu metal particle sintering) is less significant for 1Cu1Zn function. This result is explained by the role of Zn as an active spacer for decreasing the extent of Cu^{2+} reduction and Cu agglomeration [27] and is consistent with the optimum atomic ratio of Cu/Zn = 1.0:1.0 determined in the literature for this purpose [26].

The higher specific metal surface area for CZA function than for 1Cu1Zn function evidences that the incorporation of small Al amounts contributes to increasing the metal surface area, given that Cu is more easily dispersed on a support with a higher BET surface area [48]. An increase in the calcination temperature from 325 °C to 400 °C causes a significant decrease in the metal surface area for CZA function (almost half). The effect is similar for 1Cu1Zn function and lower for 2Cu1Zn function. The specific metal surface area for G66 function is 78 m^2_{Cu}/g_{Cu}.

The average Cu particle size increases as the metal surface area is decreased, and therefore its evolution by increasing the calcination temperature and adding Zn and Al is opposite to that observed for the metal surface area.

Fig. 3 shows the X-ray diffractogram pattern for the catalyst based on the CZA metallic function calcined at 325 °C. The peaks corresponding to CuO and ZnO metallic phases are observed, as are those corresponding to the crystalline structure of the zeolite, but

Table 3
Effect of the metallic function composition on the physical-chemical properties of the catalysts synthesized.

Properties	CZA/A0.2-300	1Cu1Zn/A0.2-300	2Cu1Zn/A0.2-300	G66/A0.2-300
Cu/Zn/Al nominal	4.5:4.5:1.0	1.0:1.0:0	2.0:1.0:0	3.0:1.0:1.0
Cu/Zn/Al real	4.5:4.7:1.0	–	–	–
wt% nominal metal content	50	50	50	50
wt% real metal content	49.7	50.6	49.0	50.2
S_{BET}, m^2/g	215	208	209	213
$V_{micropore}$, cm^3/g	0.05	0.05	0.05	0.05
$V_{mesopore}$, cm^3/g	0.27	0.28	0.29	0.27
d_{pore}, Å	75	80	83	70
$S_{metallic}$, $m^2{}_{Cu}/g_{Cu}$	70	54	33	48
$\bar{d}_{Cu}$, Å	96	124	203	141
Total acidity, $mmol_{NH_3}/g_{cat}$	0.36	0.35	–	–
Average acid strength, kJ/mol_{NH_3}	115	117	–	–

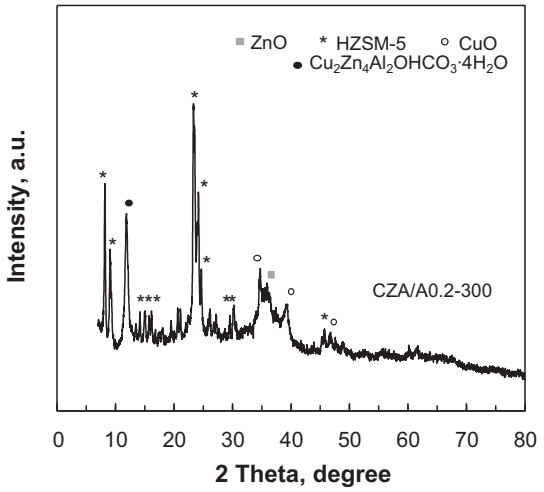

Fig. 3. XRD pattern for CZA/A0.2-300 bifunctional catalyst calcined at 325 °C.

not those corresponding to Al_2O_3 (which is probably due to a high dispersion of this phase or to its low content in the bifunctional catalyst).

The TPR profiles for the bifunctional catalysts are shown in Fig. 4. The profiles record a peak corresponding to a reduction in the Cu^{2+} phase, which is located at a higher temperature (190 °C) for CZA/A0.2-300 catalyst. This peak shifts to a lower temperature (170 °C) for G66/A0.2-300 and 1Cu1Zn/A0.2-300 catalysts.

The composition and physical-chemical properties of the bifunctional catalysts (Table 3) depend on the values of the Cu/Zn/Al

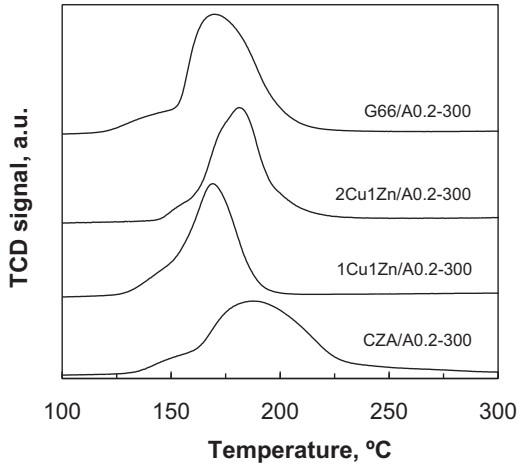

Fig. 4. TPR profiles for the catalysts prepared with different metallic functions.

atomic ratio, which are close to the nominal ones. The BET surface area of the catalysts is midway between those for the individual functions and the porous structure is bimodal, with micropores provided by the acid function and mesopores provided by both the acid and metallic functions.

Table 3 also shows that the mesopore volume for the bifunctional catalyst is slightly lower than for CZA metallic function (Table 2), and similar to that corresponding to A0.2-300 acid function [32]. Overall, the specific metal surface area for the bifunctional catalysts ($S_{metallic}$ in Table 3) is almost half that corresponding to the individual metallic functions (Table 2), which is explained by the additional calcination at 325 °C for 2 h undergone by the bifunctional catalyst, whose consequence is Cu particle agglomeration and, therefore, lower dispersion. Consequently, the specific metal surface area follows the same order as for the individual metallic functions, with the highest value being for CZA/A0.2-300 catalyst, with the smallest Cu average particle size.

The total acidity for the bifunctional catalysts (Table 3) is closely related to the real content of the acid function (50 wt%) and to the corresponding acidity (Table 1). This result shows that the total acidity of the acid function incorporated does not decrease when the preparation method studied is followed. Furthermore, there is no significant decrease in the acid strength of the sites. Moreover, no significant differences are observed between the acidity of the bifunctional catalysts prepared by using different metallic functions and, therefore, the acidity of the catalysts prepared is a direct consequence of the acid function used.

3.2. Kinetic performance of the different catalysts

3.2.1. Reaction indices

DME conversion, X_{DME}, and yield of H_2 and CO, Y_i, have been calculated as follows:

$$X_{DME} = \frac{F_{DME,0} - F_{DME}}{F_{DME,0}} \quad (7)$$

$$Y_i = \frac{F_i \cdot \upsilon_i^{-1}}{F_{DME,0}} \quad (8)$$

where F_i is the molar flow rate of the component i, which is evaluated from its molar fraction (calculated from chromatographic results) and the total molar flow rate (determined by the atomic balances of H, C and O), υ_i is the stoichiometric coefficient of the component i produced in SRD. The subscript "0" denotes the initial molar flow rate.

In order to quantify the activity of the metallic function in the bifunctional catalyst, the effective conversion of methanol has been

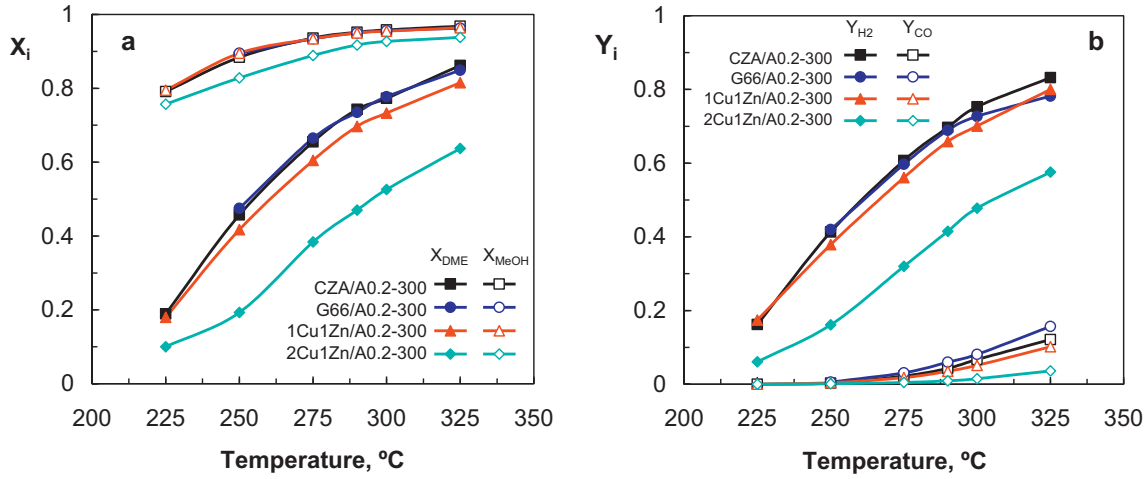

Fig. 5. Effect of temperature on DME conversion and MeOH effective conversion (graph a) and on H_2 and CO yields (graph b) for bifunctional catalysts prepared with different metallic functions. Reaction conditions: 1.2 bar, steam/DME/He molar ratio = 3:1:0.85, space time = 0.40 $g_{catalyst}$ h/g_{DME}, P_{DME} = 0.25 bar.

determined in the second step of the SRD process (i.e., methanol steam reforming, Eq. (2)), X_{MeOH}, as:

$$X_{MeOH} = \frac{F_{MeOH,0} - F_{MeOH}}{F_{MeOH,0}} \quad (9)$$

where $F_{MeOH,0}$ is the methanol molar flow rate corresponding to DME conversion, which is calculated as twice the number of DME moles converted, according to the stoichiometry of DME hydrolysis (Eq. (1)).

Hydrogen production, P_{H_2}, has been defined as the moles of hydrogen formed by time and catalyst mass unit:

$$P_{H_2} = \frac{F_{H_2}}{W} \quad (10)$$

3.2.2. *Effect of the metallic function composition on the kinetic performance of the catalyst at zero time on stream*

Fig. 5 shows the effect of temperature on the conversions of DME (Eq. (7)) and methanol (Eq. (9)) (Fig. 5a) and on the yields of H_2 and CO (Eq. (8)) (Fig. 5b). The results correspond to zero time on stream (fresh catalysts) and the same reaction conditions: pressure, 1.2 bar; steam/DME molar ratio, 3:1; space time, 0.40 $g_{catalyst}$ h/g_{DME}; partial pressure of DME (P_{DME}), 0.25 bar. It should be noted that the yield of CH_4 is insignificant, and the yield of CO_2 may be determined by subtracting the yield of CO from the conversion of DME.

As observed, the catalyst with 2Cu1Zn metallic function is the least active and selective for H_2 formation in the whole range of temperatures studied, which in view of the similar catalyst acidity is explained by the lower specific metal surface area of the catalyst prepared based on this 2Cu1Zn function (Table 3).

In the case of catalysts with a metallic function with a Cu/Zn atomic ratio of 1:1 (with or without Al in their formulation, namely, CZA and 1Cu1Zn), although they have a different metallic dispersion (Table 3) the difference in the kinetic performance is less significant, as was also observed by Kawabata et al. [20]. Nevertheless, the catalysts with Al in their metallic function (CZA prepared in the laboratory and commercial G66) are more active and both allow attaining similar levels of DME conversion and MeOH effective conversion (Fig. 5a). A comparison of H_2 and CO yields (Fig. 5b) shows that, above 250 °C and using the catalyst prepared based on G66 commercial function, the yield of CO is higher and that of H_2 lower. This result is explained by the higher content of Cu in G66 metallic function than in CZA function, which enhances the reverse water-gas shift reaction (r-WGS, Eq. (4)) at sufficiently high temperatures for this reaction to occur. It is also observed that an increase in temperature increases the yield of H_2, reaching a value of 0.83 for CZA catalyst at 325 °C.

Table 4 sets out the results for DME conversion, MeOH effective conversion and H_2 and CO molar fractions at the reactor outlet at zero time on stream for catalysts with different metallic function. These results correspond to given reaction conditions and show that the catalyst with CZA metallic function is slightly more active and selective for H_2 production than that prepared with commercial G66 metallic function, which is explained as mentioned above by a more suitable composition of CZA function, being also consistent with the results reported by Kawabata et al. [20].

The same CZA metallic function has been used with different acid functions in a previous paper [32] dealing with SRD, and the HZSM-5 zeolite desilicated under the aforementioned conditions recorded a porous structure with mesopores and suitable acid structure. The hydrolysis activity is much higher than that corresponding to γ-Al_2O_3, which allows operating at a lower temperature, with lower CO formation and without Cu sintering. Furthermore, the moderate desilication with NaOH generates mesopores in the HZSM-5 zeolite, thereby enhancing the internal diffusion of the reaction components and attenuating the acid strength, thus minimizing the capacity for hydrocarbon formation and, therefore, coke formation. Long et al. have obtained similar results by attenuating the acidity of the HZSM-5 zeolite by doping with MgO [30]. Furthermore, the presence of hexamethylbenzene in the SRD product stream [31] when HY or Hbeta zeolites are used as acid function evidences that the formation of hydrocarbons as byproducts takes place from methanol and DME through the well-reported hydrocarbon pool mechanism, in which polymethylbenzenes are intermediates retained in the porous structure. The moderate acid strength of the HZSM-5 zeolite and the small micropores play a significant role in decreasing the formation of these

Table 4
Comparison of DME conversion, MeOH effective conversion and H_2 and CO molar fractions at zero time for bifunctional catalysts prepared with different metallic functions. Reaction conditions: 300 °C, 1.2 bar, steam/DME/He = 4:1:0.55 molar, space time = 0.15 $g_{catalyst}$ h/g_{DME}, P_{DME} = 0.22 bar.

Catalyst	X_{DME}	X_{MeOH}	x_{H_2}	x_{CO}
CZA/A0.2-300	0.63	0.96	0.59	0.008
G66/A0.2-300	0.60	0.96	0.56	0.011
1Cu1Zn/A0.2-300	0.57	0.93	0.53	0.003
2Cu1Zn/A0.2-300	0.36	0.78	0.33	0.001

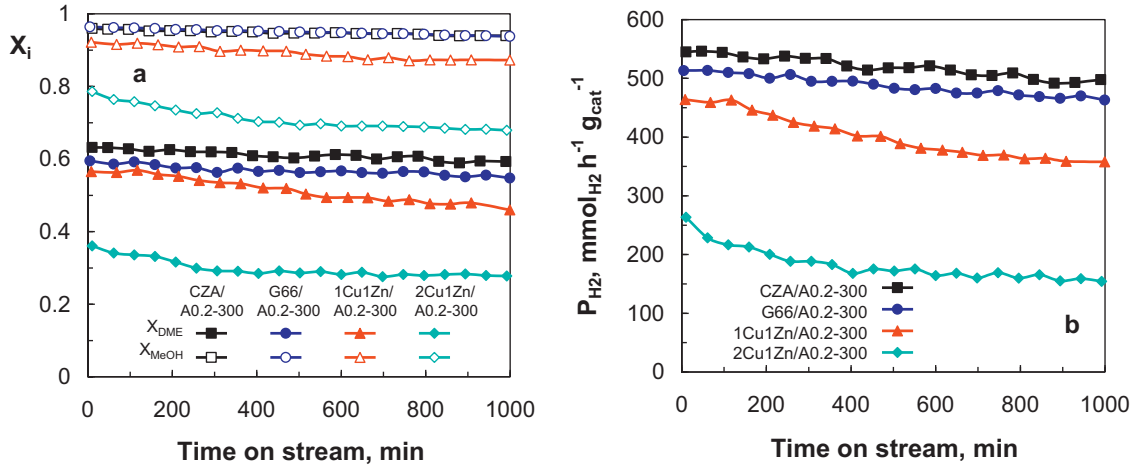

Fig. 6. Evolution with time on stream of DME conversion and MeOH effective conversion (graph a) and of H_2 production (graph b) for bifunctional catalysts prepared with different metallic functions. Reaction conditions: 300 °C, 1.2 bar, steam/DME/He molar ratio = 4:1:0.55, space time = 0.15 $g_{catalyst}$ h/g_{DME}, P_{DME} = 0.21 bar.

intermediates that reduce the yield of H_2 and are presumably coke precursors [49].

Furthermore, noble metals are an alternative to Cu catalysts. Thus, it has been proven that the use of Rh and Au catalysts supported on CeO_2 for DME reforming provides excellent results, with a high H_2 yield (87% at 500 °C, with a catalyst of 1%K + 1%Au/CeO_2 + Al_2O_3 for full conversion of DME) and significant stability [24,25].

3.2.3. *Effect of the metallic function composition on catalyst deactivation*

Fig. 6 compares the evolution with time on stream of DME conversion and methanol effective conversion (Fig. 6a), and of H_2 production (Fig. 6b) at 300 °C. The runs correspond to a space time of 0.15 $g_{catalyst}$ h/g_{DME}, which is lower than that corresponding to Fig. 5 (0.40 $g_{catalyst}$ h/g_{DME}) in order to observe clearer differences due to: (i) component concentration being further from thermodynamic equilibrium and (ii) a more significant deactivation.

The results in Fig. 6 for the evolution of reaction indices with time on stream (up to 17 h) show that all the catalysts undergo slight deactivation (reaction indices decrease slightly with time on stream). Nevertheless, as observed in Fig. 6a, CZA/A0.2-300 and G66/A0.2-300 catalysts (both containing Al in the metallic function) are more stable, with DME conversion and methanol effective conversion being similar with both catalysts. H_2 production (Fig. 6b) is slightly higher with CZA/A0.2-300 catalyst than with G66/A0.2-300 catalyst and decreases slightly with time on stream following a similar trend for both catalysts. It should be noted that the decrease in H_2 production with time on stream is more pronounced due to the simultaneous decrease in DME and methanol conversions.

The possible causes of catalyst deactivation are Cu sintering (irreversible) and coke deposition (reversible). In order to ascertain the real cause, it should be noted that combustion at 300 °C of the coke deposited on CZA/A0.2-300 catalyst allows recovering a specific metal surface area (measured by chemisorption of N_2O pulses) of 69 m^2_{Cu}/g_{Cu}, which is almost the same as that of the fresh catalyst (70 m^2_{Cu}/g_{Cu}). The combustion of the coke at such a low temperature as 300 °C means that it is a coke deposited on the metallic sites, which catalyze coke combustion. These results allow discarding sintering and attribute the cause of the deactivation to coke deposition on the metallic function, which explains why specific metal surface area of the deactivated catalyst is 57 m^2_{Cu}/g_{Cu}. This value is significantly lower than that of the fresh catalyst due to the deposition of coke on the metallic sites, which remain inaccessible for N_2O chemisorption. This hypothesis of preferential deactivation by coke on the metallic function is consistent with the kinetic results (Fig. 6a), that is, the conversions of DME and methanol decrease with time on stream. It should be noted that, in the event coke preferably deposits on the acid function, DME conversion would decrease more significantly than that of methanol.

The coke contents (determined by combustion with air) in the catalysts deactivated for 17 h (corresponding to the runs in Fig. 6) are very low: 0.05, 0.11, 0.06 and 0.10 wt% for 2Cu1Zn/A0.2-300, 1Cu1Zn/A0.2-300, CZA/A0.2-300 and G66/A0.2-300 catalysts, respectively. Nevertheless, this low content causes a significant partial blockage of the metallic sites and, therefore, a decrease in the reaction indices. The results in Fig. 6 show the significance the Al content in the metallic function has for attenuating the blockage of metallic sites by coke, which is attributed to the role of Al_2O_3 for storing the growing coke that is forming on the metallic sites. This shifting of coke precursors from the Cu surface towards the interface with Al_2O_3 has also been observed in DME synthesis on catalysts of similar composition to those used in this paper [12].

4. Conclusions

The kinetic performance in the SRD process (activity, H_2 selectivity and stability) of bifunctional catalysts depends on the Cu/Zn/Al atomic ratio of the metallic function.

The CuZnAl metallic function is obtained by coprecipitation in a reproducible way and with a suitable control of the Cu/Zn/Al atomic ratio required. The calcination of this metallic function above 300 °C fully develops the crystalline structure of the phases making up CuO and ZnO (no Al_2O_3 peaks are observed by XRD) and 250 °C is a suitable temperature for reducing all Cu species. The addition of ZnO significantly enhances CuO metal dispersion and avoids its sintering. Furthermore, the addition of a small amount of Al_2O_3 increases the BET surface area and pore volume, thereby increasing the specific metal surface area (Cu dispersion is enhanced).

Therefore, CZA metal function (synthesized in the laboratory with Cu/Zn/Al atomic ratio = 4.5:4.5:1.0) calcined at 325 °C is suitable for preparing the bifunctional catalyst for SRD, given that it is highly active, stable below 300 °C (resistant to deactivation) and gives way to low CO formation rate.

Although the coke content deposited on the catalyst is very low, deactivation is significant due to its deposition mainly on the metallic function (its combustion takes place at 300 °C because it is catalyzed by this function), which explains the decrease in methanol conversion with time on stream.

Acknowledgements

This work has been carried out with the financial support of the Ministry of Science and Technology of the Spanish Government (Projects CTQ2006-12006 and CTQ2009-13428), University of the Basque Country (UFI 11/39) and of the Basque Government (Project GIC07/24-IT-220-07).

References

[1] T.A. Semelsberger, R.L. Borup, H.L. Greene, Journal of Power Sources 156 (2006) 497–511.
[2] C. Arcoumanis, C. Bae, R. Crookes, E. Kinshita, Fuel 87 (2008) 1014–1030.
[3] T. Mathew, Y. Yamada, A. Ueda, H. Shyoyama, T. Kobayashi, C.S. Gopinath, Applied Catalysis A 286 (2005) 11–22.
[4] Y. Tanaka, R. Kikuchi, T. Takeguchi, K. Eguchi, Applied Catalysis B 57 (2005) 211–222.
[5] T. Nishiguchi, K. Oka, T. Matsumoto, H. Kanai, K. Utani, S. Imamura, Applied Catalysis A 301 (2006) 66–74.
[6] T.A. Semelsberger, K.C. Ott, R.L. Borup, H.L. Greene, Applied Catalysis A 309 (2006) 210–223.
[7] T.A. Semelsberger, K.C. Ott, R.L. Borup, H.L. Greene, Applied Catalysis B 65 (2006) 291–300.
[8] Y. Yamada, T. Mathew, A. Ueda, H. Shioyama, T. Kobayashi, Applied Surface Science 252 (2006) 2593–2597.
[9] F. Solymosi, R. Barthos, A. Kecskeméti, Applied Catalysis A 350 (2008) 30–37.
[10] N. Shimoda, K. Faungnawakij, R. Kikuchi, K. Eguchi, International Journal of Hydrogen Energy 36 (2011) 1433–1441.
[11] A.T. Aguayo, J. Ereña, I. Sierra, M. Olazar, J. Bilbao, Catalysis Today 106 (2005) 265–270.
[12] J. Ereña, I. Sierra, M. Olazar, A.G. Gayubo, A.T. Aguayo, Industrial and Engineering Chemistry Research 47 (2008) 2238–2247.
[13] I. Sierra, J. Ereña, A.T. Aguayo, M. Olazar, J. Bilbao, Industrial and Engineering Chemistry Research 49 (2010) 481–489.
[14] J. Ereña, I. Sierra, A.T. Aguayo, A. Ateka, M. Olazar, J. Bilbao, Chemical Engineering Journal 174 (2011) 660–667.
[15] W.H. Chen, B.J. Lin, H.M. Lee, M.H. Huang, Applied Energy 98 (2012) 92–101.
[16] G.A. Olah, A. Goeppert, G.K.S. Prakash, Journal of Organic Chemistry 74 (2009) 487–498.
[17] D.A. Bulushev, J.R.H. Ross, Catalysis Today 171 (2011) 1–13.
[18] K. Faungnawakij, R. Kikuchi, T. Matsui, T. Fukunaga, K. Eguchi, Applied Catalysis A 333 (2007) 114–121.
[19] T.A. Semelsberger, K.C. Ott, R.L. Borup, H.L. Greene, Applied Catalysis A 61 (2005) 281–287.
[20] T. Kawabata, H. Matsuoka, T. Shisido, D. Li, Y. Tian, T. Sano, K. Takehira, Applied Catalysis A 308 (2006) 82–90.
[21] A.T. Aguayo, J. Ereña, D. Mier, J.M. Arandes, M. Olazar, J. Bilbao, Industrial and Engineering Chemistry Research 46 (2007) 5522–5530.
[22] T. Mathew, K. Sivaranjani, E.S. Gnanakumar, Y. Yamada, T. Kobayashi, C.S. Gopinath, Journal of Materials Chemistry 22 (2012) 13484–13493.
[23] T. Fukunaga, N. Ryumon, S. Shimazu, Applied Catalysis A 348 (2008) 193–200.
[24] G. Halasi, T. Bánsági, F. Solymosi, ChemCatChem 1 (2009) 311–317.
[25] A. Gazsi, I. Ugrai, F. Solymosi, Applied Catalysis A 391 (2011) 360–366.
[26] S. Murcia-Mascarós, R.M. Navarro, L. Gómez-Sainero, U. Costantino, M. Nocchetti, J.L.G. Fierro, Journal of Catalysis 198 (2001) 338–347.
[27] M. Vijayaraj, C.S. Gopinath, Journal of Catalysis 241 (2006) 83–95.
[28] S.D. Badmaev, P.V. Snytnikov, International Journal of Hydrogen Energy 33 (2008) 3026–3030.
[29] J. Li, Q. Zhang, X. Long, P. Qi, Z.T. Liu, Z.W. Liu, Chemical Engineering Journal 187 (2012) 299–305.
[30] X. Long, Q. Zhang, Z. Liu, P. Qi, J. Lu, Z. Liu, Applied Catalysis B 134/135 (2013) 381–388.
[31] X. Long, Q. Zhang, R. Guo, Z. Liu, H. Wang, J. Lu, Z. Liu, Catalysis Today (2013), http://dx.doi.org/10.1016/j.cattod.2012.10.030.
[32] J. Vicente, A.G. Gayubo, J. Ereña, A.T. Aguayo, M. Olazar, J. Bilbao, Applied Catalysis B 130/131 (2013) 73–83.
[33] J.P. Shen, C. Song, Catalysis Today 77 (2002) 89–98.
[34] Y. Kawamura, K. Yamamoto, N. Ogura, T. Katsumata, A. Igarashi, Journal of Power Sources 150 (2005) 20–26.
[35] J. Ereña, J.M. Arandes, R. Garoña, A.G. Gayubo, J. Bilbao, Journal of Chemical Techology and Biotechnology 78 (2003) 161–166.
[36] J. Ereña, J. Vicente, A.T. Aguayo, A.G. Gayubo, M. Olazar, J. Bilbao, International Journal of Hydrogen Energy (2013), http://dx.doi.org/10.1016/j.ijhydene.2013.05.134 (in press).
[37] I. Yusta, F. Velasco, J.M. Herrero, Boletín de la Sociedad Española de Mineralogía 17 (1994) 39–50.
[38] J.W. Evans, M.S. Wainwright, A.J. Bridgewater, D.J. Young, Applied Catalysis 7 (1983) 75–83.
[39] A.G. Gayubo, A.T. Aguayo, A. Atutxa, R. Prieto, J. Bilbao, Industrial and Engineering Chemistry Research 43 (2004) 5042–5048.
[40] A.G. Gayubo, A.T. Aguayo, A. Atutxa, R. Prieto, J. Bilbao, Energy and Fuels 18 (2004) 1640–1647.
[41] I. Sierra, J. Ereña, A.T. Aguayo, J.M. Arandes, M. Olazar, J. Bilbao, Applied Catalysis B 106 (2011) 167–173.
[42] A.J. Akande, R.O. Idem, A.K. Dalai, Applied Catalysis A 287 (2005) 159–175.
[43] D. Feng, Y. Zuo, D. Wang, J. Wang, Chinese Journal of Chemical Engineering 17 (2009) 64–71.
[44] J. Agrell, M. Boutonnet, I. Melián-Cabrera, J.L.G. Fierro, Applied Catalysis A 253 (2003) 201–211.
[45] M. Shimokawabe, H. Asakawa, N. Takezawa, Applied Catalysis 59 (1990) 45–58.
[46] J.P. Breen, J.R.H. Ross, Catalysis Today 51 (1999) 521–533.
[47] B. Lindström, L.J. Pettersson, Journal of Power Sources 106 (2002) 264–273.
[48] R.M. Navarro, M.A. Peña, J.L.G. Fierro, Chemical Reviews 107 (2007) 3952–3991.
[49] M. Guisnet, L. Costa, F. Ramôa Ribeiro, Journal of Molecular Catalysis A 305 (2009) 201–211.